Heliyon 9 (2023) e21597

Contents lists available at ScienceDirect

Heliyon

journal homepage: www.cell.com/heliyon

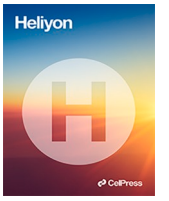

A probability distribution model for the compressive strength of micro thin-walled hollow glass beads under uniform pressure

Jingze Wang, Weicheng Cui *

Key Laboratory of Coastal Environment and Resources of Zhejiang Province, School of Engineering, Westlake University, 600 Dunyu Road, Hangzhou, 310030, Zhejiang Province, China

ARTICLE INFO

Keywords:
Hollow glass bead
Compressive strength
Probability distribution

ABSTRACT

Because of their many excellent properties, hollow glass beads (HGBs) are widely used in composite materials; stealth coatings; the aerospace field; the deep-sea field; electrical, thermal and sound insulation materials and military explosives. However, there is currently no method for predicting the strength of HGBs. This paper proposes a probability distribution model for the compressive strength of micro thin-walled HGBs under uniform pressure. The theoretical model was verified by comparing the parameters of 13 types of HGBs. The model showed that compressive strength is inversely proportional to the square root of the radius for the same type of HGBs. Moreover, for different types of HGBs made with identical materials, the compressive strength is only related to the outer diameter and equivalent density. Further study revealed that the particle size of HGBs follows a normal distribution. The failure mode of HGBs under uniform pressure is mode-II. Therefore, the maximum shear stress, which occurs on the inner surface of HGBs, is the dominant factor in the failure process. Furthermore, the shear strength is only inversely proportional to the square root of the radius even for different types of HGBs.

1. Introduction

Hollow glass beads (HGBs) have many excellent properties such as low density; high melting point; good electrical, heat and sound insulation; high temperature resistance and shrinkage resistance [1–4]. They are widely used in composite materials; stealth coatings; the aerospace field; the deep-sea field; electrical, thermal, sound insulation materials, and military explosives [5–9]. For example, HGB/epoxy resin composites prepared from HGBs are lightweight but have high compressive strength [10]. They can provide buoyancy compensation for manned/unmanned deep submersibles to enable them to float [11–13]. Their application has enabled manned submersibles to transition from the first generation (20–30 tonnes for full ocean depth) to the second generation (150 tonnes for full ocean depth) [14–16]. Therefore, they are of great significance to the exploration and development of deep-sea resources.

At present, HGBs and their composites are mainly used in the engineering field as functional materials [17,18]. Although they also have strong application prospects in load-bearing structures because of their good compressive properties, their application to such structures is progressing slowly. The main reason behind the slow progress is that there is no strength theory for HGBs and thus no theoretical basis when they are used in structural design and optimisation.

HGBs are the weak link in their composites because of their thin shells and defect sensitivity, which is due to their brittle nature [19]. Under an external load, they crack easily and become the source of cracks in the composite [20]. The cracks then expand from the

* Corresponding author.
E-mail address: cuiweicheng@westlake.edu.cn (W. Cui).

https://doi.org/10.1016/j.heliyon.2023.e21597
Received 24 November 2022; Received in revised form 13 October 2023; Accepted 24 October 2023
Available online 7 November 2023

microscale to the macroscale in the interface phase and matrix phase, finally causing the failure of the composite material [21–24]. Therefore, before applying HGBs and their composites to load-bearing structures, the failure behaviour of HGBs should be studied [25, 26].

In 1951, Hall found the following relationship between grain strength and grain size, as shown in Eq. (1):

$$\sigma_{th} = \frac{k}{d^x}, \tag{1}$$

where σ_{th} is the grain strength, d is the grain size and k is a constant. Because of technical limitations, Hall only derived a proportional relationship and did not provide the value of x. Then, Petch found that the strength is proportional to the reciprocal of the square root of the diameter, as shown in Eq. (2):

$$\sigma_{th} = \sigma_0 + \frac{k}{\sqrt{d}}. \tag{2}$$

The above formula describes the Hall–Petch effect. In this formula, σ_0 is the friction stress in the absence of grain boundaries. The Hall–Petch effect has been repeatedly shown to be applicable to grain sizes varying from 1 mm down to 1 μm [3,4]. The size of HGBs is also within this range. Therefore, this is also the limitation of the theoretical approach in this paper. However, the sizes, strengths and spatial distributions of HGBs are random [22,27], which makes it difficult to propose a compressive strength model. In this paper, assuming that the failure strength is proportional to the square root of the radius and that the fracture mode is similar to mode-II, the distribution of the compressive strength of HGBs is effectively characterised. Then, a micro-compressive strength model and its distribution model for HGBs are proposed.

2. Theoretical derivation

2.1. Basic assumptions

In 1920, Griffith proposed the theory of fracture mechanics [28], and nearly a hundred years of development by many scholars has led to the present fracture mechanics theory. Fracture mechanics proposes three modes of failure [29]: (I) tensile fracture, (II) shear fracture and (III) mixed tensile and shear fracture. However, tensile stress cannot occur in HGBs under uniform pressure. Therefore, we believe that neither mode-I nor mode-III fractures can occur and that the fracture mode of HGBs under uniform pressure is mode-II. Hence, several basic assumptions are proposed and verified by comparing the theory with experimental data. The basic assumptions are as follows:

1) The materials of HGBs are ideal elastomers.
2) HGBs form standard spheres under surface tension. Therefore, the HGBs are assumed to have no initial deformation.
3) According to the fracture mechanics theory, there are only three fracture modes. However, neither mode-I nor mode-III can occur when the HGBs are under uniform pressure. Therefore, it is assumed that the fracture mode of HGBs under uniform pressure is mode-II.
4) Experimental data show that the density HGBs with different particle sizes of the same type does not differ significantly. Therefore, the density of all HGBs of the same type is independent of particle size.
5) Characterising the shapes and sizes of the initial defects in HGBs is difficult. Therefore, it is assumed that there is an average value that can represent the effect of initial defects on the compressive strength of HGBs.

2.2. Compressive strength model

The fracture mode of HGBs under uniform pressure is shear fracture (mode-II). This means that the fracture of HGBs under uniform pressure follows the maximum shear stress criterion. According to Hall's research, the yield stress scales with the inverse square root of grain size [30–32], as shown in Eq. (3):

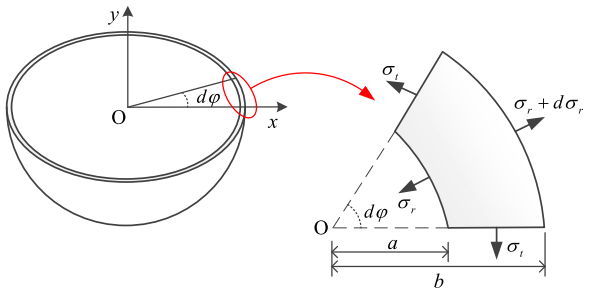

Fig. 1. The internal stresses of hollow glass bead shell.

$$\tau_{th} = \frac{k}{\sqrt{r}}, \tag{3}$$

where τ_{th} is the shear strength, r is the radius of an HGB and k is a measure of the local stress required to initiate plastic flow at a grain boundary. With a small-angle spherical shell as the research object, the internal stress of hollow glass microspheres is as shown in Fig. 1. According to the elastic theory [33], the radial and tangential normal stress distributions in the spherical shell under uniform pressure are as follows, as shown in Eq. (4):

$$\begin{cases} \sigma_r = -\dfrac{1-\dfrac{a^3}{r^3}}{1-\dfrac{a^3}{b^3}}p \\ \sigma_t = -\dfrac{1+\dfrac{a^3}{2r^3}}{1-\dfrac{a^3}{b^3}}p \end{cases}, \tag{4}$$

where a and b are the inner and outer radii of the HGBs, respectively, the radius r varies from a to b, p is the uniform pressure and σ_r and σ_t are the radial and tangential stresses, respectively. The failure of HGBs under uniform pressure is similar to mode-II. Therefore, the maximum shear stress dominates the failure process. According to the theory of material mechanics, the maximum shear stress distribution along the radial direction is as follows [33]:

$$\tau_{\max} = \frac{\sigma_r - \sigma_t}{2}, \tag{5}$$

where $\tau_{\max}$ is the maximum shear stress at any point ($a \le r \le b$). Obviously, when $r = a$, the maximum shear stress is the highest. Substituting $r = a$ into Eq. (4) yields Eq. (6):

$$\begin{cases} \sigma_r = -\dfrac{1-\dfrac{a^3}{a^3}}{1-\dfrac{a^3}{b^3}}p = 0 \\ \sigma_t = -\dfrac{1+\dfrac{a^3}{2a^3}}{1-\dfrac{a^3}{b^3}}p = -\dfrac{3}{2\left(1-\dfrac{a^3}{b^3}\right)}p \end{cases}. \tag{6}$$

Further, substituting Eq. (6) into Eq. (5) yields Eq. (7):

$$\tau_{\max} = \frac{\sigma_r - \sigma_t}{2} = \frac{1}{2}\left[0 - \left(-\frac{3}{2\left(1-\frac{a^3}{b^3}\right)}p\right)\right] = \frac{3}{4\left(1-\frac{a^3}{b^3}\right)}p(r=a) \tag{7}$$

The mass of air in the HGBs is very small and can be ignored. Therefore, the mass of glass is the mass of the HGBs, as shown in Eq. (8):

$$\begin{aligned} & m_b = m_g = \rho_g V_g \\ & \Rightarrow \rho_b V_b = \rho_g V_g \\ & \Rightarrow \frac{\rho_b}{\rho_g} = \frac{V_g}{V_b} \end{aligned}, \tag{8}$$

where m_{g} and m_{b} are the masses of glass and HGBs, respectively, ρ_{b} and V_{b} are the equivalent density and the volume of HGBs, respectively and ρ_{g} and V_g are the density and volume of glass, respectively. The volume of glass is equal to the volume of HGBs minus the volume of the hollow portion. Therefore, we obtain Eq. (9) as follows:

$$\frac{\rho_b}{\rho_g} = \frac{\frac{4}{3}\pi b^3 - \frac{4}{3}\pi a^3}{\frac{4}{3}\pi b^3} = 1 - \frac{a^3}{b^3}. \tag{9}$$

Substituting Eq. (9) into Eq. (7) yields Eq. (10):

$$\tau_{\max} = \frac{3}{4\left(\frac{\rho_b}{\rho_g}\right)}p = \frac{3}{4}\frac{\rho_g}{\rho_b}p(r=a). \tag{10}$$

Equation (10) shows the relationship between pressure and maximum shear stress for ideal elastic materials. According to Petch's research, friction stress enhances the grain tensile strength. However, in the case of compression failure, defects may cause a reduction in grain strength:

$$\begin{aligned} & p_{th} = p_0 - p_l \\ & \Rightarrow p_0 = p_{th} + p_l \end{aligned}, \tag{11}$$

where p_{th} is the pressure corresponding to the fragmentation of HGBs, p_0 is the fracture strength of the ideal elastic material and p_l is the strength loss due to defects. Obviously, p in Eq. (10) corresponds to p_0. Substituting Eq. (11) into Eq. (10) yields Eq. (12):

$$\begin{aligned} & \tau_{th} = \frac{3}{4}\frac{\rho_g}{\rho_b} p_0 \\ & \Rightarrow \tau_{th} = \frac{3}{4}\frac{\rho_g}{\rho_b}\left(p_{th} + p_l\right), \\ & \Rightarrow p_{th} = \frac{4}{3}\frac{\rho_b}{\rho_g}\tau_{th} - p_l \end{aligned} \tag{12}$$

where τ_{th} is the maximum shear stress when an HGB cracks. Substituting Eq. (3) into Eq. (12) yields Eq. (13):

$$p_{th} = \frac{4}{3}\frac{\rho_b}{\rho_g}\frac{k}{\sqrt{r}} - p_l. \tag{13}$$

For the same type of HGBs, the equivalent density is assumed to be equal. Therefore, by defining $K_1 = \frac{4k\rho_b}{3\rho_g}$, Eq. (12) can be simplified as follows:

$$p_{th} = \frac{K_1}{\sqrt{r}} - p_l. \tag{14}$$

However, different types of HGBs with identical materials and production processes have different equivalent densities. Therefore, by defining $K_2 = \frac{4k}{3\rho_g}$, we can simplify Eq. (14) as follows:

$$p_{th} = K_2\frac{\rho_b}{\sqrt{r}} - p_l. \tag{15}$$

Equations (14) and (15) reflect the compressive strength models of HGBs. They show that the compressive strength of HGBs made of identical materials depends only on their outer radius and equivalent density (related to wall thickness). In particular, the compressive strength of the HGBs is directly proportional to the equivalent density and inversely proportional to the square root of their outer radius.

2.3. Probability distribution model of compressive strength

Equations (14) and (15) can be used to predict the compressive strength of a single HGB. However, when HGBs are applied to engineering, their number is usually very large. Therefore, the probability distribution of the strength of HGBs is worth studying. For the same type of HGBs, it is simpler to use Eq. (14):

Table 1
Hollow glass beads and their parameters.

Series	Kinds	Density (g/cm^3)	radii (μm)				p_{th}(0.9) (MPa)
			r(0.1)	r(0.5)	r(0.9)	Max	
Routine series	K1	0.125	15	32.5	55	60	1.72
	S15	0.15	12.5	27.5	45	47.5	2.07
	K20	0.20	15	32.5	55	60	3.45
	XLD3000	0.23	7.5	15	20	/	20.69
	K25	0.25	12.5	27.5	47.5	52.5	5.17
	S38HS	0.38	7.5	20	37.5	42.5	37.92
	VS5500	0.38	7.5	20	37.5	42.5	37.92
	im16K	0.46	6	8	10	/	110.32
Floating series	A16/500	0.16	17.5	35	57.5	67.5	3.44
	A20/1000	0.20	15	30	50	60	6.90
	H20/1000	0.20	15	30	50	60	6.90
	D32/4500	0.32	10	20	35	42.5	31.03
	H50/10000	0.50	10	20	25	30	68.95

$$p_{th}=\frac{K_1}{\sqrt{r}}-p_l \Rightarrow r=\left(\frac{K_1}{p_{th}+p_l}\right)^2 r\in[r_{\min},r_{\max}]. \tag{16}$$

Tests showed that the particle size of HGBs approximately followed a normal distribution. Therefore, we obtain the following:

$$\begin{aligned}&\frac{r-\mu}{\sigma}\sim N(0,1)\\&\Rightarrow f(r)=\frac{1}{\sqrt{2\pi}\sigma}\exp\left(-\frac{(r-\mu)^2}{2\sigma^2}\right)\end{aligned}, \tag{17}$$

where $f(r)$ is the probability density function and μ and σ are the average and standard deviation of the outer radius, respectively; they are listed in Table 1. Then, the cumulative probability distribution function is as follows:

$$\Phi(r)=\frac{1}{\sqrt{2\pi}\sigma}\int_{r_{\min}}^{r}\exp\left(-\frac{(r-\mu)^2}{2\sigma^2}\right)dr. \tag{18}$$

from Eq. (16),

$$r=\left(\frac{K_1}{p_{th}+p_l}\right)^2 \Rightarrow dr=-\frac{2{K_1}^2}{(p_{th}+p_l)^3}dp_{th}. \tag{19}$$

Substituting Eq. (19) into Eq. (17) yields the probability density function of compressive strength for the HGBs:

$$f(p_{th})=\frac{1}{\sqrt{2\pi}\sigma}\exp\left(-\frac{\left(\left(\frac{K_1}{p_{th}+p_l}\right)^2-\mu\right)^2}{2\sigma^2}\right). \tag{20}$$

Further, substituting Eq. (19) into Eq. (18) yields the cumulative probability distribution for the HGBs:

$$\Phi(p_{th})=-\frac{{K_1}^2}{\sigma}\sqrt{\frac{2}{\pi}}\int_{\frac{K_1}{\sqrt{r_{\min}}}+p_l}^{\frac{K_1}{\sqrt{r}}+p_l}\frac{1}{(p_{th}+p_l)^3}\exp\left(-\frac{\left(\left(\frac{K_1}{p_{th}+p_l}\right)^2-\mu\right)^2}{2\sigma^2}\right)dp_{th}. \tag{21}$$

Equations (20) and (21) reflect the compressive strength distribution models of HGBs. They represent the probability density distribution and cumulative probability distribution of compressive strength.

3. Model verification

3.1. Research objects

In this section, the relationships among the densities, particle size distributions and strengths of 13 groups of HGBs are evaluated. Then, the compressive strength model and distribution model of HGBs are verified. The HGBs were provided by Minnesota Mining and Manufacturing (3 M). The size distributions, densities, compressive strength and other parameters of HGBs given in Table 2 were

Table 2
Mean radii and standard deviations of all hollow glass beads.

Series	Kinds	Normal distribution parameters	
		Average	Standard deviation
Routine series	K1	35.00	15.61
	S15	28.75	12.68
	K20	35.00	15.61
	XLD3000	13.75	4.88
	K25	30.00	13.66
	S38HS	22.50	11.70
	VS5500	22.50	11.70
	im16K	8.00	1.56
Floating series	A16/500	37.50	15.60
	A20/1000	32.50	13.66
	H20/1000	32.50	13.66
	D32/4500	22.50	9.75
	H50/10000	17.50	5.85

provided by 3 M. In Table 2, $r(0.1)$, $r(0.5)$ and $r(0.9)$ are the quantiles of the radius for 10 %, 50 % and 90 % HGBs, respectively.

To confirm the reliability of the data provided by 3 M, XLD3000, im16K and H50/10000 were selected as the research objects. A small number of these three types of HGBs were used to prepare observation samples, and photos were taken under a scanning electron microscope (SEM). Nano Measurer 1.2 software was used to measure the particle size of each glass bead in the SEM photos (see Fig. 2). The measured quantities of XLD3000, im16K and H50/10000 were 940, 900 and 900, respectively. The quantity distributions of the different particle sizes are shown in the histograms in Fig. 3(a–c).

3.2. Particle size distributions

The particle size of HGBs was assumed to follow a normal distribution. The mean radii and standard deviations of all HGBs were calculated according to the data in Table 2; the results are presented in Table 1. Then, the probability density distributions of the particle sizes of XLD3000, im16K and H50/10000 were calculated; the results are presented in the curves in Fig. 3(a–c). The curves show good agreement with the histograms, validating the reasonableness of the assumption that the particle size of HGBs follows a normal distribution.

The probability density function and cumulative probability function of all 13 types of HGBs were calculated according to Eqs. (13) and (14); the results are shown in Fig. 4(a and b). In the cumulative probability distribution (Fig. 4(b)), $r(0.1)$, $r(0.5)$ and $r(0.9)$ were calculated theoretically; they are shown in Fig. 5 and compared with the data in Table 2. In Fig. 5, -E and -T following $r(0.1)$, $r(0.5)$ and $r(0.9)$ are the abbreviations for the experimental data and theoretical values, respectively. Fig. 5 shows that there is little difference between the theoretical values and experimental data, and deviations are acceptable. This also verifies the rationality of using a normal distribution to characterise the particle size distribution of HGBs.

3.3. Compressive strength distributions

To verify the compressive strength model of HGBs, comparing the different types of HGBs is necessary. Therefore, Eq. (11) is more appropriate. Equation (11) shows that the compressive strength of HGBs is directly proportional to $\frac{\rho_b}{\sqrt{r}}$. Then, $K_2 = 868.00$ (Pa $m^{1/2}$)/(kg/m^3) and $p_l = 15.94$ MPa in this equation are calculated from the data in Table 2. In Fig. 6, the horizontal axis is $\frac{\rho_b}{\sqrt{r(0.9)}}$ and the vertical axis is $p_{th}(0.9)$. $p_{th}(0.9)$ denotes the quantile of the compressive strength of 90 % HGBs. The curves in Fig. 6 are approximately straight lines. The comparison results are in good agreement, which verifies the reliability of the compressive strength model.

The probability density distribution and cumulative probability distribution of compressive strength were calculated according to Eqs. (16) and (17), respectively. The results are presented in Fig. 7(a and b) $p_{\mathrm{th}}(0.9)$ can be calculated theoretically according to the cumulative probability distribution (Fig. 7(b)). As depicted in Fig. 8, the comparison between the theoretical values and experimental data for $p_{\mathrm{th}}(0.9)$ shows little difference. This verifies the compressive strength distribution model of HGBs.

4. Analysis

4.1. Deviation analysis

The basic assumption that HGBs follow a normal distribution may be inconsistent with the facts. Fig. 4 shows that when the particle size is $r \leq 0$, the probability of HGBs is $P\{r \leq 0\} > 0$, which is obviously inconsistent with the fact that the outer diameter should be $r > 0$. Taking K1 as an example yields the following:

$$\begin{cases} P\{r \leq 0\} = 1.242\% \\ P\{r \leq 30\} = 10\% \end{cases}. \tag{22}$$

Equation (22) shows that in the calculation process, the probability of $r \leq 30$ μm is 10 %. However, the actual value range of HGBs is

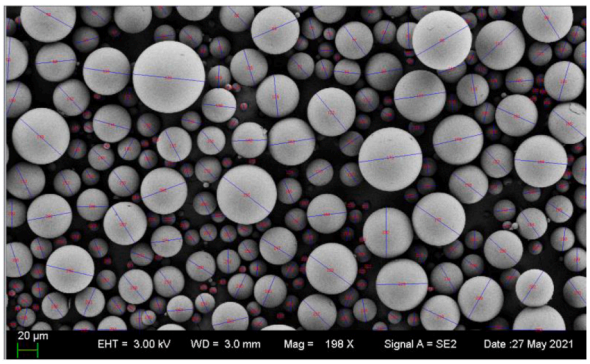

Fig. 2. Measurement of the particle size of hollow glass beads in the SEM photos.

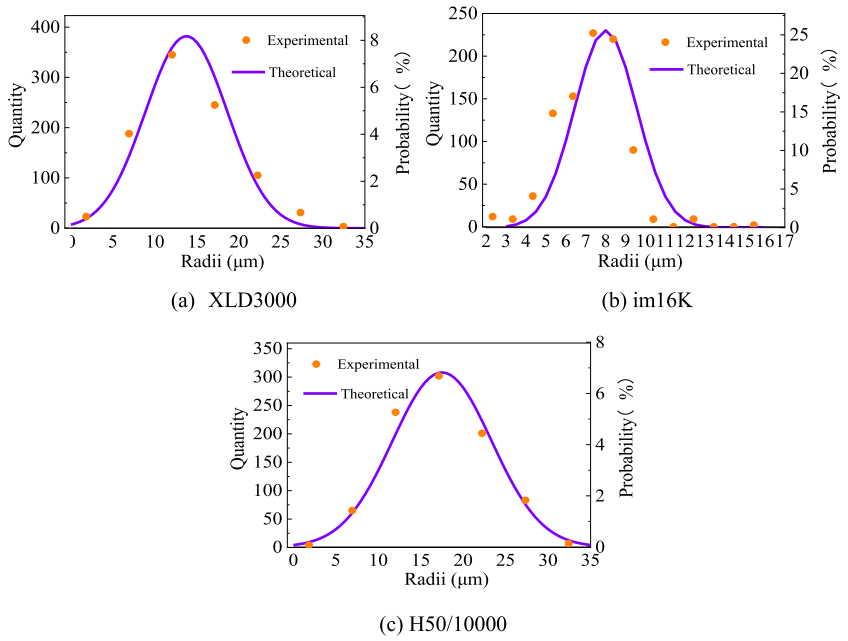

Fig. 3. Particle size distribution of three kinds of hollow glass beads.

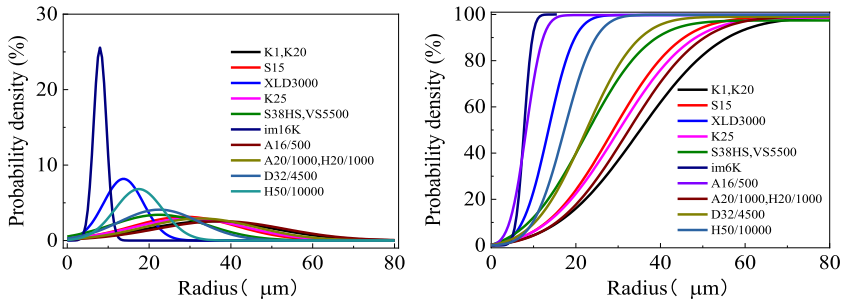

Fig. 4. Particle size probability distribution.

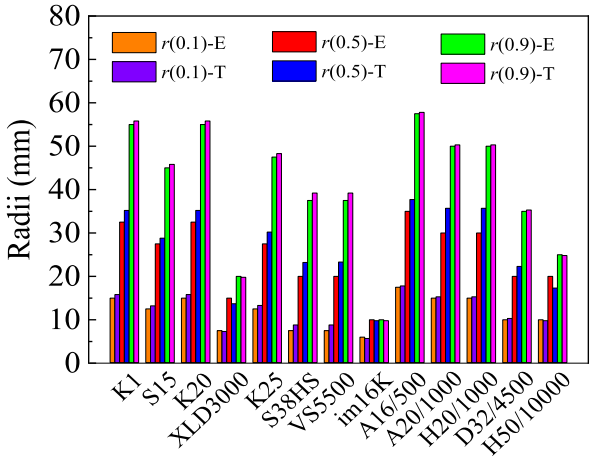

Fig. 5. Comparison between theoretical values and experimental data for $r(0.1)$, $r(0.5)$ and $r(0.9)$.

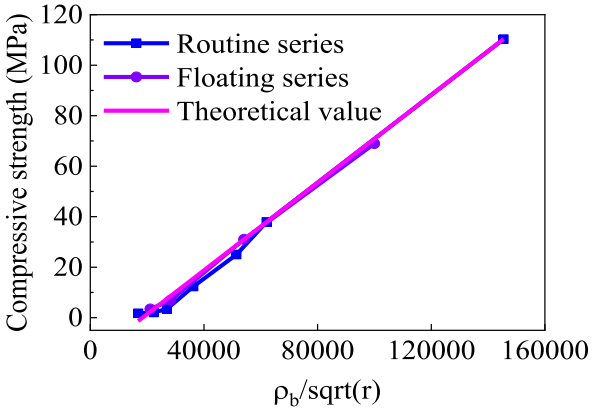

Fig. 6. Relationships among compressive strength, particle size and equivalent density.

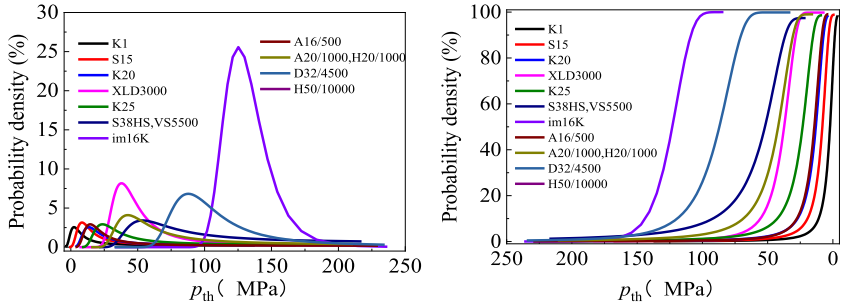

(a)The probability density distribution (b) The cumulative probability distribution

Fig. 7. Compressive strength probability distribution.

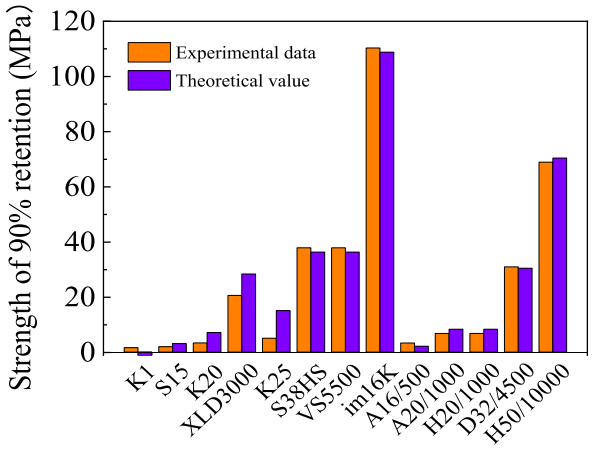

Fig. 8. Comparison between theoretical values and experimental data for $p_{th}(0.9)$.

$0 < r \leq 30$ μm. Therefore, the real probability is $P\{0 < r \leq 30\} = 10\% - 1.242\% = 8.758\%$, which will inevitably cause calculation deviations in the process. Fig. 9 shows the probabilities for all types of HGBs when $r \leq 0$. These can also be considered deviations. In Fig. 9, the probabilities for S38HS and VS5500 are the maximum, $P\{r \leq 0\} = 2.732\%$, while that for im16K is the minimum, $P\{r \leq 0\} = 0.009\%$. In addition, incomplete samples, differences in the preparation processes and the basic assumption that the same types of HGBs have a constant equivalent density can also cause deviations.

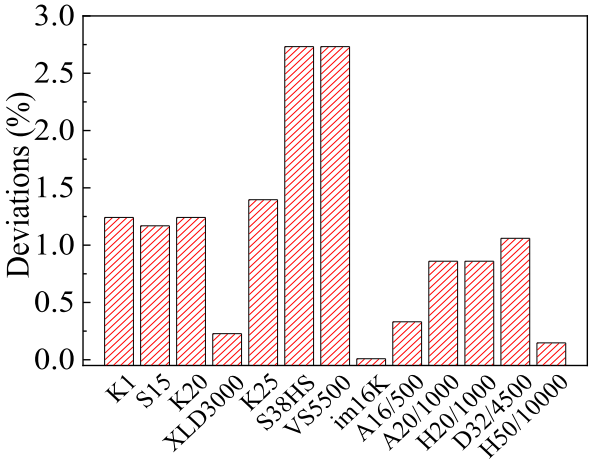

Fig. 9. Deviations of hollow glass beads caused by $r \leq 0$.

4.2. Finite element simulation and analysis

As shown in Fig. 9, the deviations of XLD3000, im16K and H50/10000 are small compared to those of other types of HGBs. Therefore, these three types of HGBs were selected as research objects. Then, finite element models of the three types of HGBs were built using ABAQUS, a powerful finite element engineering simulation software. After establishing the finite element models, the solver in ABAQUS was used to automatically calculate the stress distributions. In these finite element models, the outer diameter was the average value of HGBs, and the inner diameter was calculated according to the average density. The fragmentation strengths of these three HGB models were calculated by using Eq. (15). Then, they were applied to the model surface as uniform loads. All the parameters required by the finite element model are listed in Table 3.

The finite element model, which is a 1/8 model of HGBs, is shown in Fig. 10. The global coordinate system adopted is the rectangular coordinate system. Further, for stress and strain calculation, the spherical coordinate system is adopted. The boundary conditions are shown in Fig. 10. The three sides are symmetrical about the X, Y and Z axes of the rectangular coordinate system. A uniform pressure is applied to the outer surface.

The distributions of the radial and tangential stress obtained by the theoretical model and finite element simulation are depicted in Fig. 11(a and b), which shows that they are essentially coincident. This also verifies the theoretical model. The tangential normal stress is much larger than the radial normal stress. When $r = a$, the radial normal stress is 0. At this moment, tangential stress may be the main factor that causes the HGBs to fracture. Equation (4) shows that the radial and tangential stresses are related to the third power of the radius. However, Fig. 11(a and b) show that the tangential and radial stress curves are approximately straight lines. This is because the shell of HGBs is very thin, and the curvature of normal and shear stress changes very slightly.

The maximum shear stress distributions obtained by the theoretical model (-T) and finite element simulation (-F) are depicted in Fig. 12, which shows that the maximum shear stress in the thin shell is approximately linear. When $r = a$, the maximum shear stress is the maximum. Therefore, the initial crack occurs on the inner surface. Substituting Eq. (15) into Eq. (12) yields Eq. (23):

$$\tau_{th} = \frac{3}{4}\frac{\rho_g}{\rho_b}\left(K_2\frac{\rho_b}{\sqrt{r}}\right) = \frac{3\rho_g}{4}\frac{K_2}{\sqrt{r}}. \tag{23}$$

in Eq. (23), even for different types of HGBs, K_2 and ρ_g are constants. This means that the shear strength is only inversely proportional to the square root of the radius. The scale coefficient is k. Further, the K_1, K_2, k and strength parameters of all HGBs were calculated; these are listed in Table 4. These parameters can provide references for the design of HGBs and their composites.

According to the basic assumptions, the density of all HGBs of the same type is a constant that is independent of particle size. However, there is also a slight difference in density even for the same type of HGBs. When XLD3000, im16K and H50/10000, whose outer diameter is the average particle size and inner diameter is variable, were selected as research objects, the density varied between 0.1 and 0.6 g/cm^3. The relationship between fragmentation strength and density is shown in Fig. 13, which reveals that the fragmentation strength of HGBs has a linear relationship with the density when the outer diameter is constant.

5. Summary and conclusions

This paper proposes a compressive strength model and the probability density distribution and cumulative probability distribution of compressive strength for HGBs under uniform pressure. The theoretical model was verified by comparing the parameters of 13 types of HGBs provided by a 3 M representative. The models showed that compressive strength is inversely proportional to the square root of the radius for the same type of HGBs. In addition, the model revealed that for different types of HGBs made with identical materials, the compressive strength is only related to the outer diameter and equivalent density (related to wall thickness). Further, the particle size

Table 3
The material parameters of XLD3000, im16K and H50/10000.

HGB	E (GPa)	μ	ρ (g/cm^3)	b (μm)	a (μm)	p_{th} (MPa)
XLD3000	60.00	0.23	2.18	13.75	13.25	37.90
im16K				8.00	7.39	125.23
H50/10000				17.50	16.04	87.81

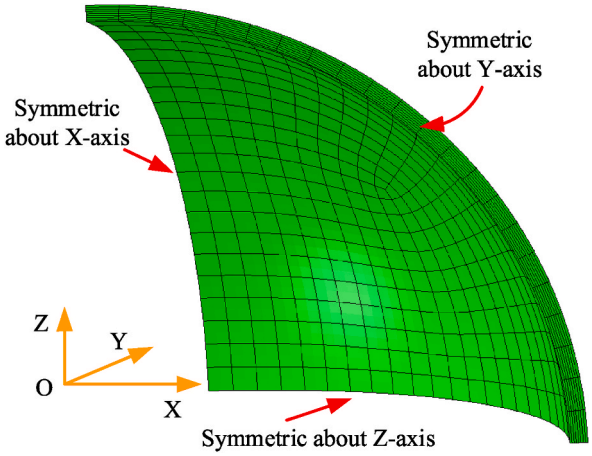

Fig. 10. The 1/8 finite element model of hollow glass beads.

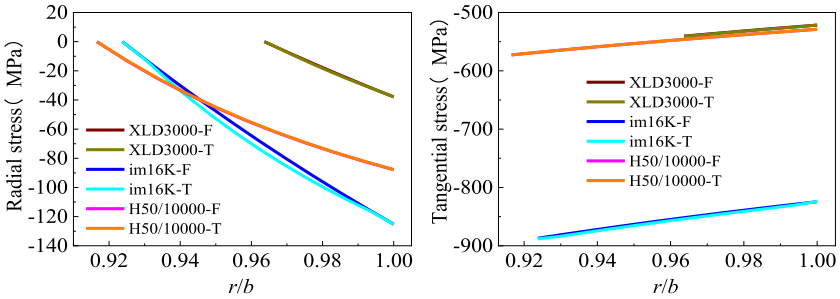

(a) The radial stress (b) The tangential stress

Fig. 11. Radial and tangential stress distributions.

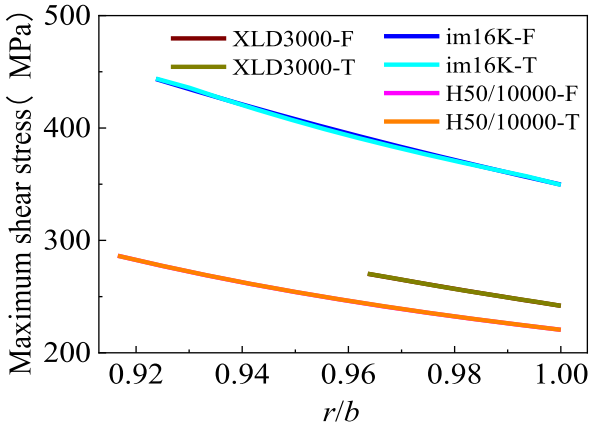

Fig. 12. Maximum shear stress distribution.

Table 4
The parameters in theoretical models.

Kinds	p_{th} (MPa)	τ_{th} (MPa)	k (Pa·m$^{1/2}$)	K_1(Pa·m$^{1/2}$)	K_2((Pa·m$^{1/2}$)/(kg/m^3))
K1	2.40	239.89	1419180	108500	868
S15	8.34	264.68	1419180	130200	868
K20	13.40	239.89	1419180	173600	868
XLD3000	37.90	382.72	1419180	199640	868
K25	23.68	259.11	1419180	217000	868
S38HS	53.60	299.19	1419180	329840	868
VS5500	53.60	299.19	1419180	329840	868
im16K	125.23	501.76	1419180	399280	868
A16/500	6.74	231.75	1419180	138880	868
A20/1000	14.51	248.94	1419180	173600	868
H20/1000	14.51	248.94	1419180	173600	868
D32/4500	42.62	299.19	1419180	277760	868
H50/10000	87.81	339.25	1419180	434000	868

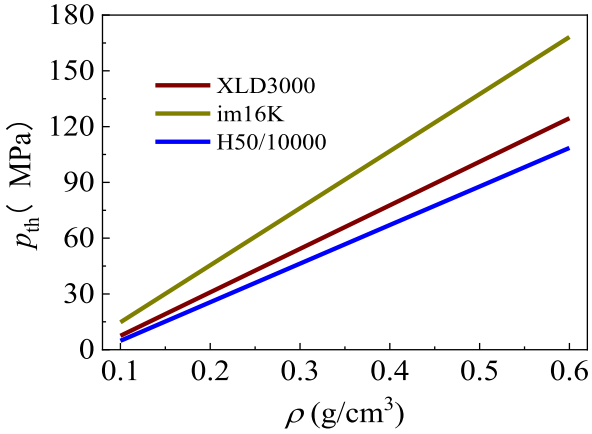

Fig. 13. Relationship between fragmentation strength and density.

of HGBs follows a normal distribution.

The reasons for deviations were analysed. Then, XLD3000, im16K and H50/10000 were taken as the research objects, and the distribution law of stress in thin shells was evaluated. The range of their inner diameters are shown in Table 5. This evaluation revealed that the failure mode of HGBs under uniform pressure is mode-II and that the maximum shear stress is the dominant factor in the failure process. Moreover, the maximum shear stress was found to occur on the inner surface of HGBs and strengthening the inner surface helped to improve the compressive strength of HGBs. Further study showed that the shear strength is only inversely proportional to the square root of the radius even for different types of HGBs.

Some parameters of HGBs were calculated, which can provide references for the design of HGBs and their composites. The relationship between fragmentation strength and density was studied, revealing that the fragmentation strength of HGBs has a linear relationship with the density when the outer diameter is constant.

Funding statement

This work is supported by the General Program of National Natural Science Foundation of China 'Study on water absorption characteristics of buoyancy material in full ocean depth manned submersible' (Grant No.51879157), the National Natural Science Foundation of China for Youth Science Project 'Mechanism of stress-moisture-creep coupling on compressive strength of composites in deep-sea' (Grant No.11902288).

Table 5
The range of inner diameters for XLD3000, im16K and H50/10000.

HGB	b (μm)	a_{min} (μm)	a_{max} (μm)	k_2
XLD3000	13.75	12.35	13.54	234082.19
im16K	8.00	7.19	7.88	306884.34
H50/10000	17.50	15.72	17.23	207491.69

Data availability statement

Data will be made available on request.

Additional information

No additional information is available for this paper.

CRediT authorship contribution statement

Jingze Wang: Investigation, Formal analysis, Conceptualization. **Weicheng Cui:** Project administration, Funding acquisition.

Declaration of competing interest

The authors declare that they have no known competing financial interests or personal relationships that could have appeared to influence the work reported in this paper.

References

[1] Y. Guo, Z. Cao, D. Wang, et al., Improving the friction and abrasion properties of nitrile rubber hybrid with hollow glass beads[J], Tribol. Int. 101 (2016) 122–130.
[2] G.B. Carvalho, S.V. Canevarolo, J.A. Sousa, Influence of interfacial interactions on the mechanical behavior of hybrid composites of polypropylene/short glass fibers/hollow glass beads[J], Polym. Test. 85 (2020), 106418.
[3] X. Quan, R. Han, Y. Shao, et al., Effect of hollow glass beads on density and mechanical properties of silicone rubber composites[J], J. Appl. Polym. Sci. 138 (7) (2021), 49865.
[4] N.B. Jackson, C.M. Wang, Z. Luo, et al., Attachment of TiO_2 powders to hollow glass microbeads: activity of the TiO_2-coated beads in the photoassisted oxidation of ethanol to acetaldehyde[J], J. Electrochem. Soc. 138 (12) (1991) 3660.
[5] S.C. Kim, D.K. Lee, Preparation of TiO2-coated hollow glass beads and their application to the control of algal growth in eutrophic water[J], Microchem. J. 80 (2) (2005) 227–232.
[6] P. Xiao, Z. Yifeng, W. Peng, et al., Estimation of thermal conduction in hollow-glass-beads-filled cement-based composites by variational asymptotic homogenization method[J], Appl. Therm. Eng. 161 (2019), 114191.
[7] B. Kang, X. Lu, J. Qu, et al., Synergistic effect of hollow glass beads and intumescent flame retardant on improving the fire safety of biodegradable poly (lactic acid)[J], Polym. Degrad. Stabil. 164 (2019) 167–176.
[8] X. Hu, H.S. Xu, Z.M. Li, Morphology and properties of poly (L-lactide)(PLLA) filled with hollow glass beads[J], Macromol. Mater. Eng. 292 (5) (2007) 646–654.
[9] T. Huang, C.G. Ma, P.B. Dai, et al., Improvement in dielectric constant of carbon black/epoxy composites with separated structure by surface-modified hollow glass beads with reduced graphene oxide[J], Compos. Sci. Technol. 176 (2019) 46–53.
[10] M. Le Gall, D. Choqueuse, P.Y. Le Gac, et al., Novel mechanical characterization method for deep sea buoyancy material under hydrostatic pressure[J], Polym. Test. 39 (2014) 36–44.
[11] F. Wang, K. Wang, W.C. Cui, A simplified life estimation method for the spherical hull of deep manned submersibles[J], Mar. Struct. 44 (4) (2015) 159–170.
[12] B.B. Pan, W.C. Cui, C. Ye, et al., Development of the unpowered diving and floating prediction system for deep manned submersible "JIAOLONG"[J], J. Ship Mech. 18 (20) (2012) 2379–2385.
[13] E.C. Hobaica, S.D. Cook, Composite buoyancy material, US Patent 3 (437) (1971) 622.
[14] W.Q. Feng, D.Z. Wei, C. Xian, et al., Preparation and characterization of solid buoyancy materials based on epoxy resins[J], Fine Chem. (2005).
[15] X. Dong, M. Wang, X. Tao, et al., Properties of heat resistant hollow glass microsphere/phosphate buoyancy materials with different coatings[J], Ceram. Int. 46 (1) (2020) 415–420.
[16] T. Von Kármán, H.S. Tsien, The buckling of thin cylindrical shells under axial compression[J], J. Aeronaut. Sci. 8 (8) (1941) 303–312.
[17] S. Ren, X. Hu, H. Ren, et al., Development of a buoyancy material of hollow glass microspheres/SiO2 for high-temperature application[J], J. Alloys Compd. 721 (2017) 213–219.
[18] Y. Niu, S. Wang, Z. Zhu, et al., Robust composite aerogels with excellent flame retardant and thermal insulation properties based on modified hollow glass microspheres[J], Polym. Degrad. Stabil. 202 (2022), 110030.
[19] E.M. Wouterson, F.Y. Boey, X. Hu, S.C. Wong, Specific properties and fracture toughness of syntactic foam: effect of foam microstructures, Compos. Sci. Technol. 65 (11–12) (2005) 1840–1850.
[20] E.M. Wouterson, F.Y.C. Boey, X. Hu, et al., Specific properties and fracture toughness of syntactic foam: effect of foam microstructures[J], Compos. Sci. Technol. 65 (11–12) (2005) 1840–1850.
[21] N. Gupta, R. Nagorny, Tensile properties of glass microballoon-epoxy resin syntactic foams[J], J. Appl. Polym. Sci. 102 (2) (2006) 1254–1261.
[22] L. Bardella, A. Sfreddo, C. Ventura, et al., A critical evaluation of micromechanical models for syntactic foams[J], Mech. Mater. 50 (2012) 53–69.
[23] L. Bardella, Mechanical Behavior of Glass-Filled Epoxy Resins: Experiments, Homogenization Methods for Syntactic Foams, and applications[M], Université de Brescia, 2000.
[24] V.A. Buryachenko, M. Brun, FEA in elasticity of random structure composites reinforced by heterogeneities of non canonical shape[J], Int. J. Solid Struct. 48 (5) (2011) 719–728.
[25] N. Gupta, R. Ye, M. Porfiri, Comparison of tensile and compressive characteristics of vinyl ester/glass microballoon syntactic foams[J], Compos. B Eng. 41 (3) (2010) 236–245.
[26] A. Sfreddo, C. Ventura, Comparison of Models for the Effective Moduli of Syntactic Foams on the Base of Finite Element Simulations, Laurea Specialistica Thesis, University of Brescia, Italy, 2011.
[27] H.S. Kim, P. Plubrai, Manufacturing and failure mechanisms of syntactic foam under compression[J], Compos. Appl. Sci. Manuf. 35 (9) (2004) 1009–1015.
[28] A.A. Griffith, VI. The phenomena of rupture and flow in solids[J], Philos. Trans. R. Soc. Lond. - Ser. A Contain. Pap. a Math. or Phys. Character 221 (1921) 163–198, 582–593.
[29] S.K. Maiti, Fracture Mechanics: Fundamentals and applications[M], Cambridge University Press, 2015.
[30] E.O. Hall, The deformation and ageing of mild steel: III discussion of results[J], Proc. Phys. Soc. B 64 (9) (1951) 747.
[31] N.J. Petch, The cleavage strength of polycrystals[J], J. Iron Steel Inst. 174 (1953) 25–28.
[32] A. Lasalmonie, J.L. Strudel, Influence of grain size on the mechanical behaviour of some high strength materials[J], J. Mater. Sci. 21 (1986) 1837–1852.
[33] M.H. Sadd, Elasticity: Theory, Applications, and numerics[M], Academic Press, 2009. Fig. captions.